Solenoid-free startup experiments in DIII-D

2011 Nucl. Fusion 51 063038

(http://iopscience.iop.org/0029-5515/51/6/063038)

Nucl. Fusion **51** (2011) 063038 (11pp) doi:10.1088/0029-5515/51/6/063038

Solenoid-free startup experiments in DIII-D

J.A. Leuer[1], G. Cunningham[2], D. Mueller[3], N.H. Brooks[1], N.W. Eidietis[1], D.A. Humphreys[1], A.W. Hyatt[1], G.L. Jackson[1], J. Lohr[1], P.A. Politzer[1], R.I. Pinsker[1], R. Prater[1], P.L. Taylor[1], M.L. Walker[1], R.V. Budny[3], D.A. Gates[3], A. Nagy[3], S-H. Hahn[4], Y-K. Oh[4], S-W. Yoon[4], J.H. Yu[5], M. Murakami[6], J.M. Park[6] and A.C. Sontag[6]

[1] General Atomics, PO Box 85608, San Diego, CA 92186-5608, USA
[2] EURATOM/CCFE Fusion Association, Culham Science Centre, Abingdon, OX14 3DB UK
[3] Princeton Plasma Physics Laboratory, P.O. Box 451, Princeton, NJ 08543, USA
[4] National Fusion Research Institute, Daejeon 305-333, Korea
[5] UC San Diego, 9500 Gilman Dr., La Jolla, CA 92093, USA
[6] Oak Ridge National Laboratory, 1 Bethel Valley Road, Oak Ridge, TN 37831, USA

Received 12 January 2011, accepted for publication 12 April 2011
Published 20 May 2011
Online at stacks.iop.org/NF/51/063038

Abstract
A series of DIII-D experiments was performed to investigate the potential for initiating plasma current using only poloidal field coils located outside the DIII-D central solenoid, i.e. 'solenoid-free'. Plasma current to 166 kA was achieved using 2–3 MW of electron cyclotron (EC) heating and was limited by coil and power supply constraints. Flux conversion to plasma current was similar to standard DIII-D startup with some degradation at higher plasma current associated with stray fields and vertical stability issues. In preliminary solenoid-free experiments, neutral beam (NB) current drive (CD) levels were small and attributed to reduced CD efficiency associated with low electron temperature produced by the low current, low confinement plasma. Lack of plasma radial position control also contributed to a reduction of NBCD. Similarly, ECCD was small owing to low plasma temperature and outside EC launch which is required in the solenoid-free scenario. Synergistic experiments were carried out using standard solenoid initiated plasmas in order to study noninductive CD in limited, Lmode plasmas, typical of that generated by solenoid-free startup. While substantial noninductive current can be driven, self-sustaining levels of noninductive current have not yet been achieved with our present six-source co-injection NB system combined with EC and fast wave systems. At low plasma current and high levels of localized EC heating, substantial MHD is generated and this was seen to severely limit plasma performance. Although further optimization is possible in the limited plasma regime, full noninductive, steady-state operation may require diverted plasma with H-mode quality confinement. Discharges obtained during the solenoid-free campaign are compared with results of previous DIII-D campaigns aimed at achieving a steady state, noninductive CD solution.

(Some figures in this article are in colour only in the electronic version)

1. Introduction

Over the past few years, substantial research has been devoted to the development of the tokamak path to fusion energy [1]. One candidate topology for this mission is the low aspect ratio concept typified by the spherical tokamak (ST) [2] and a primary need for success of this concept is plasma initiation without a central solenoid (CS) [3–10]. Solenoid-free startup has been addressed to varying degrees using [3–11]: coaxial helicity injection (CHI), electron cyclotron heating (ECH), point source helicity injection and electron Bernstein waves (EBW). Many smaller scale experiments in CDX-U [12, 13], HIT [3], LATE [14], TST-2 [15] and QUEST [16] have provided valuable insight into the various noninductive radio-frequency (RF) techniques for tokamak startup. Notable inductive experiments using nonsolenoidal coils were performed in MAST generating 400 kA using in-vacuum vessel coils and the merging-compression technique [8, 9] and in JT-60U achieving 100 kA of solenoid-free operation using only outer poloidal field (PF) coils [10–11]. Experiments in NSTX have achieved CHI startup and coupling to an inductive current ramp-up with a current savings of approximately 200 kA [17]. A notable DIII-D experiment achieved steady-state current of

340 kA in an H-mode, high poloidal beta (β_p) plasma using eight co-injected neutral beam (NB) sources of hydrogen injecting into a helium plasma with handoff from a standard ohmic startup [18]. With six co-injected deuterium (D) NB sources injected into a D plasma, the lowest steady-state, noninductive plasma current produced in DIII-D is 600 kA and this was obtained in a highly controlled, diverted, H-mode plasma following a conventional ohmic startup [19]. Finally, preliminary scenario development work for solenoid-free operation of DIII-D utilizing divertor and outer PF coils was performed by W.P. West and R.R. Khayrutdinov[7] and the present scenario contains many attributes from these studies.

In this paper, we explore startup of the DIII-D tokamak using PF coils located outside the centrepost region and with strong ECH assist. This is potentially the most advantageous method for solenoid-free startup since no new PF system components are needed and nothing is needed inside the vacuum chamber. Two synergistic experimental campaigns were performed during the 2009–2010 run periods to quantify the potential of solenoidless startup in DIII-D. The first was purely 'solenoid-free' and established the maximum plasma current achievable within the present DIII-D coil and power supply (PS) limits. The second campaign used our standard startup with handoff to fully noninductive current drive (CD) to evaluate potential for steady-state CD at the low currents typical of the solenoid-free startup. Section 2 describes the solenoid-free scenario design and constraints imposed by the DIII-D PS system. Section 3 describes results of the solenoid-free campaign, which implemented three scenarios of progressively increasing current generation potential and risk. Section 4 documents preliminary solenoid-free noninductive CD experiments and results of the second campaign focused on obtaining noninductive CD using conventional startup in limited plasmas. Section 5 compares the present experiments with a limiter configuration to results of several previous DIII-D campaigns which utilized well controlled, diverted, H-mode plasmas to attain noninductive CD. Section 6 provides conclusions and methods for improving the DIII-D solenoid-free startup.

2. DIII-D Solenoid-free scenario design

Figure 1 shows the overall geometry of the DIII-D device [20]. DIII-D has a flexible PF coil system consisting of a distributed electric field (E-coil) system and a field shaping (F-coil) system, composed of 18 independent coils distributed around the vacuum vessel. The E-coil, with its large voltage capability and uniform flux generation capability, in combination with the outer two F-coil pairs (F6, F7), is used in conventional ohmic startup [7, 21]. Plasma heating and CD are provided by NB [22], ECH [23] and fast wave (FW) [24] systems. Three co-directed NBs with two sources each are available for CD. The three 'right' sources intersect the tangential to the vacuum system axis at 47° and provide maximum CD. The 'left' sources have 63° angles with the axis, are less efficient at CD and primarily provide heating. Each source is capable of providing approximately 2.5 MW of injected power at full injector voltage (~80 kV) [22]. A total of approximately

[7] West W.P. *et al* 1997 Intl Workshop on the *Spherical Torus '97 (St. Petersburg, Russia, 3–5 September)* (http://www.ioffe.rssi.ru/STWS97/).

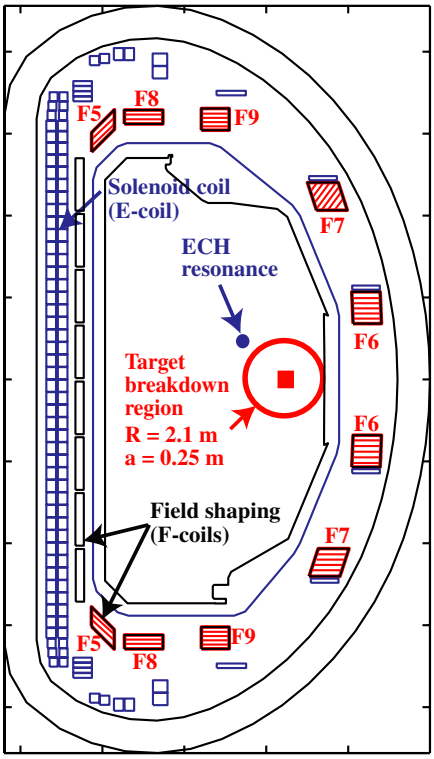

Figure 1. DIII-D cross-section showing major axisymmetric magnet systems. The PF coil system is composed of the E (Electric) and F (Field shaping) coil systems and is used for normal plasma initiation. For solenoid-free startup, only coil pairs F5–F9 (above/below the midplane, crosshatched) are used for plasma initiation. Circle represents the plasma target. The ECH resonance is shown.

3 MW of 110 GHz ECH is available through 5–6 gyrotron tubes [23]. A fast wave current drive (FWCD) system, with approximately 3.5 MW at 60 or 90 MHz [24], is also available.

The DIII-D PF coil system was designed to provide large flexibility in plasma shaping. However, as in most other devices [8–11], operation in a solenoid-free configuration requires substantial system modification and introduces unique constraints not present in normal startup operations. In the DIII-D solenoid-free experiments, many of the PF coils were disabled. The E-coil and inner F-coil stack were not utilized. Only F-coil pairs F5–F9 (divertor and vertical field coils, red hatched in figure 1) are used for solenoid-free startup. This required significant modification of our typical electrical configuration and introduced a number of constraints that are not typically present in our normal E/F-coil system. In particular, the F-coil PS system uses DC PSs connected to silicon-controlled rectifiers (SCRs) chopper units and provide a pulse width modulated (PWM) output voltage to each coil. This system does not permit zero crossing of coil current, which in turn limits our null/flux generation potential. In addition, maximum negative voltage is required for solenoid-free startup and this requires shutting off the positive voltage part of the pulse and relying only on the $I \times R$ voltage drop of the resistor for output, significantly reducing any active control capability. In the experiment, most of these coils (F5, F6, F8 and F9) were operated at their maximum negative voltage capability and generated a null centred electric field of approximately 0.4 V m^{-1}. Only coil F7 was under active

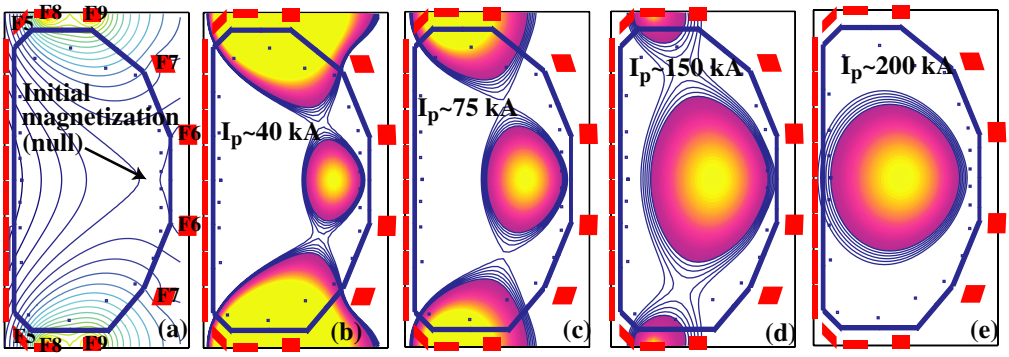

Figure 2. Solenoid-free scenario development equilibrium flux plots (FIESTA). Frame (*a*) shows the IM null formation state prior to plasma initiation. (*b*)–(*e*) The evolution of plasma current transfer from the PF coils with (*e*) the final maximum plasma current state.

control to either follow a prescribed coil current trajectory or, later in the campaign, provide plasma radial feedback control. The ECH system resonance location for full toroidal field operation is above and inside of the null formation region as shown in figure 1. This location is dictated by line-of-site geometrical constraints which is associated with launching port interactions and leads to loss of ionized particles along the field lines and reduced heating during the critical plasma initiation phase compared with that which can be generated by a null centred resonance location.

The design approach used for the DIII-D solenoid-free startup scenario development is similar to that successfully applied to EAST [25, 26] and KSTAR [26] and envisioned for ITER [27]. Plasma sequences were established for the solenoid-free scenario based on the equilibrium code FIESTA[8], a free-boundary Grad–Shafranov equilibrium code, which used approximate flux states expected in the discharge. Figure 2 shows a sequence of flux plots representative of projected plasma behaviour based on preliminary scenario development work. The first panel shows the null formation associated with the initial magnetization (IM) flux state just prior to discharge initiation. Null and plasma formation is towards the outside of the machine (R, $a \sim 2.1$, 0.25 m). Its location is dictated by the need to thread flux through the centre of the machine while minimizing stray fields, maximizing connection length [28] and maintaining proximity to ECH resonance. Plasma equilibrium flux contours are shown in the remaining frames of figure 2 as current is extracted from the PF coils and, by Lenz' law, transferred to the plasma. The overall flux state of each equilibria was established based on projections from the initial flux state taking into account resistive losses typical of DIII-D discharges. The last frame represents the peak plasma current state when all divertor coil currents are extinguished and the plasma is maintained only by the outside vertical field coils.

Optimum startup requires an IM state that produces maximum flux and minimum stray fields, corresponding to a uniform flux plateau in the plasma initiation region just prior to plasma breakdown [27]. In the DIII-D solenoid-free configuration, this is best achieved using maximum current in the divertor coils (F5, F8, F9) and negative current in F7 with small positive current in F6 to negate the fields in the plasma region. Essentially the divertor coils and the F7 coil form a current dipole to create a null similar to that described in [26]. The quality of this null and the magnitude of flux produced dictate overall startup performance. Figure 3 shows an analysis of the relevant IM variables for solenoid-free startup in DIII-D. Plotted is the minimum average poloidal field $\langle B_P \rangle$ in the breakdown region ($R_0 = 2.1$ m, $a = 0.25$ m) for a given central flux (Φ_0). Best startup performance occurs at high IM flux ($\Phi_0 \sim$ large) and low stray fields ($\langle B_P \rangle \sim$ small), corresponding to the lower right corner in the plot. For example, the full E/F-coil system in DIII-D can achieve $\Phi_0 \sim 6$ V s with $\langle B_P \rangle \ll 10$ G over much of the vacuum vessel. The best that can be achieved in the solenoid-free DIII-D configuration lies in the regions above the two curves based on whether F6 can be used to reduce stray fields. Positive current in F6 provides the best solution (minimum $\langle B_P \rangle$ at

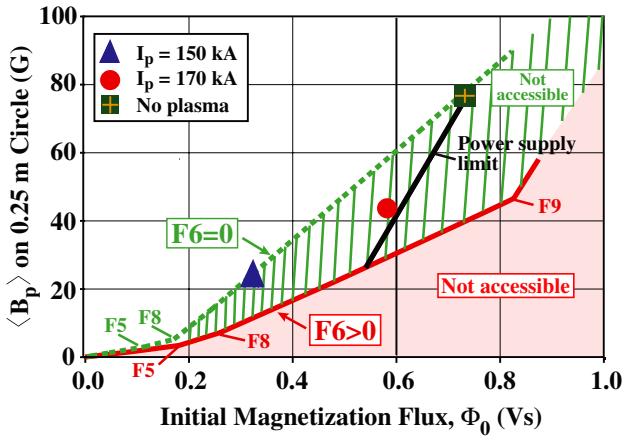

Figure 3. Calculation of DIII-D solenoid-free IM central flux versus average stray field on the breakdown circle (figure 1) under ideal conditions. Two curves represent maximum flux per unit stray field for different conditions imposed on F6 coil current: red/grey (solid line) for F6 > 0 and green (dashed line) F6 = 0. Coloured regions shown below each curve are not accessible based on constraints imposed on F6 (red shaded for F6 > 0 and green crosshatched for F6 = 0). Coil labelling in the figure (demarcated by F5, F8, F9) represents the point on the curve where the coil current reaches its maximum engineering limit. To the right of this point along each curve, the coil current is saturated at its respective limit. The IM states for several discharges are shown: 150 kA, triangle = shot 136613; 170 kA, circle = 136805; no plasma, square = 136806). Limits imposed by the PS system is shown by the solid black line and operation to the right of this line is prohibited.

[8] Cunningham G. computer code FIESTA (MAST).

a given Φ_0) and this limit is shown as the solid red (grey) curve. Normally one would want to start with positive current in F6 and drive the current negative to provide vertical field for the final plasma equilibrium. Negative current in F6 is essential for generating diverted, elongated plasma. However, our nonzero crossing constraint prohibits this and F6 = 0 is the best we can achieve in the IM state (green dashed path in figure) assuming we need F6 < 0 later in the discharge. This option leads to approximately a factor of two increase in stray plasma fields for similar flux generation. As we progress from low flux, low stray fields to higher values (left to right along the lines in figure 3), F-coil numbers are shown as each coil reaches its respective engineering current limit. It can be seen that the inner divertor coil (F5) reaches its limit first followed by the other divertor coils (F8 ⇒ F9) as we progress to higher values of flux. This indicates that the optimum solution (one with lowest stray field per central flux) favours currents placed close to the central axis. This is similar to the conventional (solenoid) solution where optimum current distribution requires largest current placed in the solenoid and close to the machine axis. Also shown in the figure is a PS limit associated with the total number of high voltage choppers, which were available during the campaign. Increase in the number of choppers available would allow us to reach higher initial flux values and, potentially, provide higher plasma current generation capability. The figure also shows several IM states (triangles and square) from our experimental discharges. These experimental points lie off the intrinsic limit lines (solid red and dashed green (grey) curves) since initial vertical field was varied to experimentally optimize plasma formation. The triangle and circle in the figure represent favourable plasma formation discharges while the square represents a failed plasma attempt.

Plasma equilibrium and stability during the early stages of plasma formation are equally important in scenario development [25, 26]. The vertical field ramp rate $\dot{B}_z$ must match the plasma current ramp rate $\dot{I}_\mathrm{p}$ which is controlled by PF coil loop voltage production. Additionally, the vertical field decay index n ($= -R_\mathrm{p}/B_z \partial B_z/\partial Z$, = curvature of the vacuum field) must remain within the stable region ($0 < n < 1.5$) [29]. Based on simple 0D plasma modelling [26] and the DIII-D PF/PS constraints we can estimate these parameters as we move away from the IM state. The DIII-D PF system can easily achieve the $\dot{B}_z$ requirements when moving off of either curve in figure 3. Stable decay index ($n \sim 1$) can be achieved by moving off of IM states with F6 > 0 (red curve). However, the power system is unable to produce a stable decay index when starting from F6 = 0 IM state (green dashed curve) and only vertically unstable plasma ($n < 0$) is possible. In particular, high initial current in the divertor coils tries to elongate the plasma ($n < 0$), while negative F7 and positive F6 counteract this to make the plasma oblate ($n > 0$). Null formation for the F6 = 0 case (green dashed curve) requires a reduction in the magnitude of both F7 and F6, and results in more current trying to elongate the plasma ($n < 0$). Experimental results with F6 = 0 are consistent with these calculations, with little plasma current generated.

The amount of plasma current achievable in the DIII-D solenoidless configuration can be estimated based on circular plasma formulation and dimensionless plasma parameters

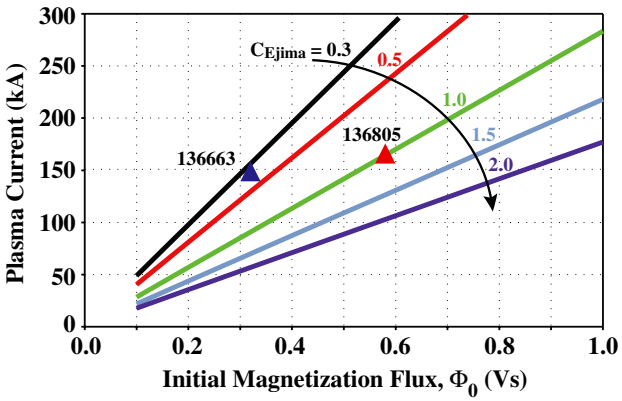

Figure 4. Variation of peak plasma current with resistive loss coefficient (C_Ejima) [30] for the DIII-D solenoidless configuration based on simple circular plasma formulation [26] and limits imposed by the machine. The results are based on equation (1) with final full-bore plasma parameters ($R_\mathrm{p} = 1.69$ m, $a = 0.67$ m, $\ell_i = 1$, $\beta_\mathrm{p} = 1$) and all equilibrium fields produced by F7. All current in the other PF coils is assumed to have decayed to zero. Results from two of our successful solenoidless discharges are also shown.

[25, 26]. Maximum plasma current is achieved when all currents are extinguished from the divertor coils and only vertical field from the outer PF coils (F7) maintains equilibrium. The current can be expressed as a function of the IM flux (Φ_0), the final plasma parameters and F7 magnetic coupling coefficients as [26]

$$I_\mathrm{p} = \frac{-\Delta\Phi}{R_\mathrm{p}\mu_0(\hat{L}_\mathrm{p} + C_\mathrm{Ejima})} = \frac{\Phi_0/(R_\mathrm{p}\mu_0)}{\left[\hat{L}_\mathrm{p} + C_\mathrm{Ejima} - \frac{\bar{\Phi}_\mathrm{F7}}{4\pi R_\mathrm{p}^2 \bar{B}_{z\mathrm{F7}}}\hat{B}_z\right]}, \quad (1)$$

where I_p is the plasma current, R_p the final plasma major radius, $\Delta\Phi$ the flux change, Φ_0 the initial flux, $\hat{L}_\mathrm{p} \equiv \{\ln[8R_\mathrm{p}/(a\sqrt{\kappa}] + (\ell_\mathrm{i}/2) - 2\}$ the dimensionless inductance, $\hat{B}_z \equiv \hat{L}_\mathrm{p} + \beta_\mathrm{p} + 1/2$ the dimensionless vertical field, a the final plasma minor radius, κ the elongation, ℓ_i the internal inductance, β_P the poloidal beta, C_Ejima the Ejima resistance coefficient $\equiv \Delta\Phi_R/(\mu_0 I_\mathrm{p} R_\mathrm{p})$, $\Delta\Phi_R$ the resistive flux [30] and $\bar{\Phi}_\mathrm{F7}/\bar{B}_{z\mathrm{F7}}$ the flux/vertical field ratio from F7 to final plasma.

Figure 4 shows predicted plasma current variation with IM flux as a function of the plasma resistive loss coefficient, C_Ejima [30]. The final equilibrium is expected to be a full bore, circular plasma with parameters ($R_\mathrm{p} = 1.69$ m, $a = 0.67$ m, $\ell_\mathrm{i} \sim 2$, $\beta_\mathrm{P} \sim 1$), maintained only by current in F7, a requirement of the current DIII-D F-coil power system. Normal ohmic startup in DIII-D has $C_\mathrm{Ejima} \sim 0.5$ (red line) and the lowest flux consumption achieved in DIII-D startup, using large inputs of ECH and NB, corresponds to $C_\mathrm{Ejima} = 0.3$ (black line). Two of the experimental solenoidless discharges are shown with the lower flux discharge (136663) approaching the best flux conversion efficiency of our normal DIII-D discharges.

3. Solenoid-free experimental results

Three primary scenarios were investigated in the solenoid-free campaign. The first two scenarios used positive current in F6, resulting in low stray fields. The first scenario used lower IM flux (0.32 V s) relative to the more aggressive, second scenario,

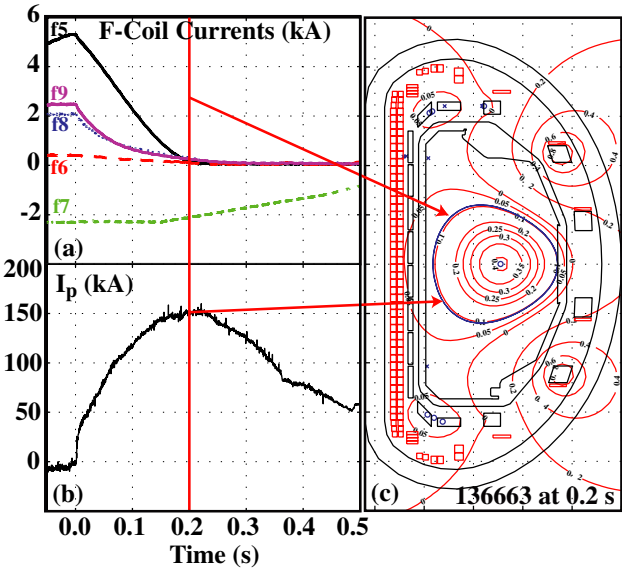

Figure 5. PF coil current (*a*), plasma current time traces (*b*), and flux map at peak current (*c*) for the conservative scenario. The decay of the divertor coil currents (F5, F8 and F9) induces plasma current, which peaks when divertor currents are exhausted. Plasma reaches maximum of 150 kA at 200 ms with F7 providing the primary vertical field for plasma equilibrium after this time. (*c*) EFIT [31] flux map indicates the plasma is outside limited. Also between 200 and 360 ms two co-source NBs were injected.

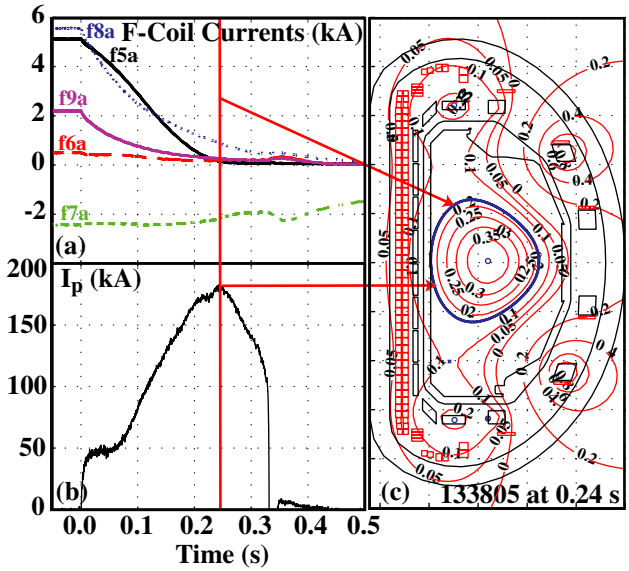

Figure 6. PF coil current (*a*), plasma current time traces (*b*) and flux map (*c*) for the aggressive scenario. The decay of the divertor coil currents (F5, F8 and F9) induce a peak plasma current of 166 kA at 240 ms. Current in F7 is providing the primary vertical field for plasma equilibrium after the peak current. The EFIT [31] flux map shown in panel (*c*) indicates the plasma is compressed onto the inside limiter at this time. At subsequent times the plasma collapses on the centrepost.

which used higher IM flux (0.58 V s) and resulted in larger stray fields. Both of these scenarios produced reasonable plasma current with the conservative scenario yielding excellent flux to plasma current conversion efficiency and the aggressive scenario achieving record current of 166 kA. The third scenario used zero initial current in F6 to allow F6 to have negative current after plasma formation, had the highest IM flux (0.74 V s) but the largest stray fields, and was projected to be vertically unstable for the first 50 ms of the discharge ($n < 0$). We were unsuccessful at generating significant current with this scenario. In all cases, the power supplies for the divertor coils (F5, F8, F9) were operated at the maximum voltage capability essentially relying on the chopper resistance to induce the voltage required for plasma initiation. The primary variables used to optimize startup were the initial vertical field established at the IM state using F7 current and the F7 coil current trajectory during plasma formation. Variations were necessary relative to the scenario predictions to compensate for eddy currents in the vacuum vessel and to optimize the experimental plasma current and radial position trajectories. All control was open loop, with only coil current in F7 under active current control. Radial position feedback was not used in the initial campaign, but was implemented at the end of the final campaign. In all cases, high gyrotron power (~2.5–3 MW injected) was needed for successful startup.

Figure 5 shows the time history of toroidal currents and the plasma equilibrium flux at peak current for the conservative scenario. The plasma current reaches 150 kA at 200 ms as all diverter coil currents (F5, F8, F9) are exhausted. The F7 coil provides the primary vertical field, which rises in the plasma as the divertor coil currents are lost. At peak current the final equilibrium is outside limited and this remains the case for the entire discharge as seen in figure 5(*c*). NBs were added at the peak current time (200 ms) and this caused a rapid outward motion of the plasma (discussed below). This scenario provided the best flux conversion efficiency for the solenoid-free campaigns. Based on EFIT [31], flux conversion to current efficiency [30] is $C_{\mathrm{Ejima}} \sim 0.33$ compared with the best achieved in DIII-D's ECH startup at ~0.3 [7].

Figure 6 shows the time history of toroidal currents and the plasma equilibrium flux at peak current for the aggressive scenario. This scenario, with its higher IM flux state, was more difficult to initiate than the conservative scenario. Flattening in plasma current seen early in the discharge (figure 6(*b*)) reflects this difficulty. It is believed that additional stray fields, more vertically unstable initial fields, and less connectivity between the ECH resonance point and plasma (figure 1) were responsible for the early losses occurring in the plasma. This scenario provided the maximum plasma current achieved, 166 kA at 240 ms, but some of this current was attributable to the compression of the plasma on the inner wall, which occurred prior to the peak current. The flux map at peak current (figure 6(*c*)) shows the plasma inside limited and well inside the chamber centre. Coil F8 has significant current even at the time of maximum plasma current. Based on EFIT reconstructions, the plasma becomes diverted just prior to the current peak as the plasma transitions from outside to inside limited plasma and this indicates that it may be possible to generate a diverted plasma if some current is maintained in the upper divertor coils. The final current ramp down occurs as the vertical field from F7 is approximately held constant and the plasma compresses to small radius on the centrepost. Unlike the conservative scenario, considerable flux conversion efficiency was lost with a predicted C_{Ejima} value of 1.1 at the peak current. Most of this

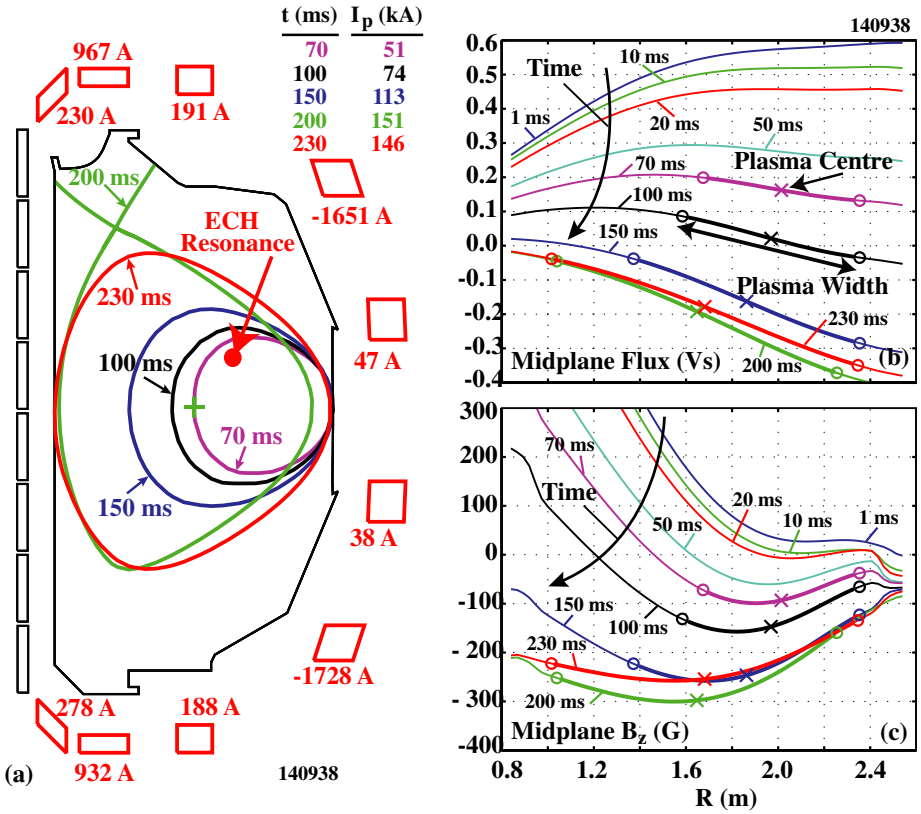

Figure 7. Typical DIII-D solenoidless evolution of (*a*) plasma shape, (*b*) midplane flux and (*c*) midplane vertical field. Shot 140938 had R_p feedback control enabled at 150 ms to centre the plasma. Shapes in (*a*) are based on EFIT with peak current occurring at 200 ms as the plasma diverts (green/grey). ECH resonance is shown in the figure and approximately 3 MW from six gyrotrons was injected up until 240 ms in the discharge. In panels (*b*) and (*c*), the x's represent the plasma centre at the midplane and the o's represent the extent of the plasma at the midplane (inner and outer boundary), based on EFIT reconstructions. The plasma is seen to grow from a small outboard circle to a diverted plasma at peak current and a full-bore plasma at slightly lower current.

was lost in the first 50 ms when flux input was maximum but the current rise rolled off.

The anatomy of the discharge shape and midplane flux and fields are shown in figure 7 for one of the discharges which included active plasma feedback control of radial position using the F7 coils. Full capability of the ECH system (6 gyrotrons, ∼3 MW) was needed for initial breakdown and burn-through. ECH power was only available until 230 ms and active radial position control was utilized after 150 ms to maintain the plasma approximately centred in the machine. The plasma evolves from a small outboard limited circle to an upper diverted plasma at peak current of 151 kA and to a full aperture limited plasma current with 146 kA at 230 ms. The currents at the full aperture plasma are shown in the figure, along with the ECH resonance location. Midplane flux and field are plotted against radius in the other frames in this figure and represent the vacuum field quantities from the PF coils, including eddy currents predicted for the vacuum vessel. Early times ($t < 50$ ms) represent the initial plasma formation stage and are prior to our ability to generate converged EFITs. For later stages, ($t >\sim 70$ ms) EFIT provides both shape and internal plasma information. The actual EFIT value for plasma radial extent ($R - a < r < R + a$) is shown with circles demarking the plasma edge and Xs the plasma centre. The plasma formation stage occurs under a favourable vertical field gradient ($\mathrm{d}B_z/\mathrm{d}r > 0$) as can be seen in panel (*c*). A negative vertical field ($B_z < 0$) and positive derivative of vertical field ($\mathrm{d}B_z/\mathrm{d}r > 0$) are needed to ensure stable plasma growth and this can be seen occurring between times 10 and 20 ms in panel (*c*). Small plasma current is observed earlier than this time and is an attribute of high ECH allowing for plasma formation over a wider range of B-field and field decay index than a conventional ohmic startup. Overall flux utilization can be determined approximately from panel (*b*) as the difference in flux at the IM state (represented by the 1 ms time) and the value at the plasma centre (denoted Xs in figure) at the peak current (200 ms). A total flux swing of approximately 0.75 V s is needed to produce the 150 kA, diverted plasma at 200 ms. The transition from the diverted plasma to the full bore-limited plasma at 230 ms shows a reduction in overall flux and is primarily a consequence of the reduction in current as the plasma transitions from diverted to limited mode.

Only equilibrium trajectories that meet the vertical stability limit ($n > 0$) were experimentally shown to produce appreciable current. This is especially true for the high flux state cases which required precise plasma conditions for current initiation. Figure 8 shows stability trajectories as defined at the breakdown location ($R = 2.1$ m, $z = 0$) for all plasma discharges that resulted in appreciable plasma current ($I_{MAX} \geqslant 150$ kA). Lines of constant decay index are shown in the figure. In the figure, initial plasma growth ($I_p < 20$ kA) is seen to occur in a narrow window of vertical field ($|B_z| < 50$ G)

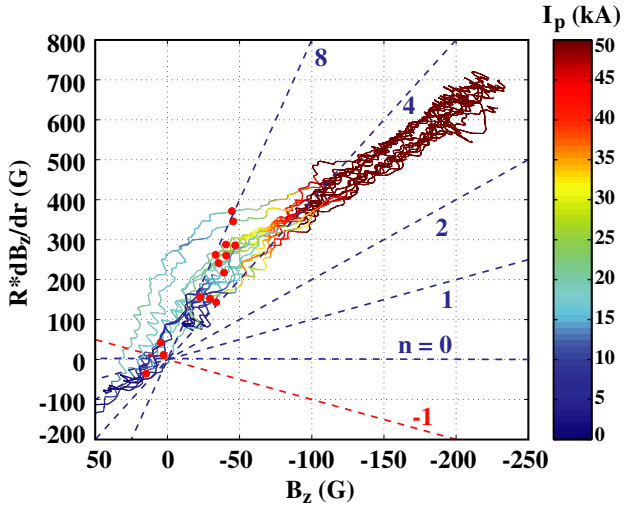

Figure 8. Stability characteristics of all successful solenoid-free discharges ($I_{pMAX} \geqslant 150$ kA). Vacuum vertical field (B_z) and radius normalized vertical field gradient ($R\,\mathrm{d}B_z/\mathrm{d}r$) are evaluated at the breakdown location ($R = 2.1$ m, $z = 0$) during each discharge. The influence of the vacuum vessel eddy currents is included in the data. Each trajectory represents discharge time from $t = 0$ to 0.2 s and in each discharge current exceeds 100 kA at the end point. Various lines of constant decay index [$n = -(R/B_z)\mathrm{d}B_z/\mathrm{d}r$] are shown in the figure with the vertically unstable ($n < 0$ [29]) line shown in red. Red dots represent approximate plasma formation time as determined from rapid increase in plasma current and levels of ECE in the region of the breakdown exceeding 50 eV for all times to peak current.

and decay index ($n > 2$). The red dots in the figure represent the time at which substantial plasma current growth is seen and the electron cyclotron emission (ECE) in the plasma breakdown region grows rapidly and exceeds 50 eV. Success of plasma formation typically occurs in the first 50 ms of the discharge and is representative of approximately $B_z \sim -50$ G in the figure. The red dots show that moderately large decay index ($n > 2$) is needed for successful startup. All discharges with low or negative decay index during the initial phase of plasma formation failed and these failures are believed to be a consequence of unstable vertical plasma motion expected in vacuum fields with negative decay index [25–28].

4. Current drive

A limited number of solenoid-free discharges were devoted to noninductive studies using NBCD and ECCD. To explore ECCD, two discharges with almost identical plasma properties and EC power input but with radial launch (heating or ECH) and oblique launch (co-CD or ECCD) showed almost identical peak plasma current (~160 kA). Both discharges had similar electron temperatures (~1 keV) as measured by Thomson and ECE and similar confinement times, ($\tau_E \sim 2$–10 ms), based on total injected power. Overall EC heating rather than CD seems to be most important for plasma current generation in the early stages of solenoid-free plasma development. Figure 9 shows plasma parameters for a solenoid-free initiated discharge with two co-directed, left (most tangential) NB sources injecting 5.1 MW of power just after peak plasma current (200 ms). EC power in the ECCD direction is injected with four gyrotrons at the 2 MW level. When NB injection starts (200 ms), the divertor PF coil currents (F5, F8, F9) are exhausted (figure 5) and no more inductive flux is added to the system. Plasma current is sustained at 150 kA for ~30 ms and is associated with the transient nature of the current redistribution following beam injection. The sustainment is attributable to changes in ℓ_i and β_P and influence of external vertical field during this nonstationary transition. The introduction of beams caused large changes in plasma parameters, many of which are detrimental to sustained plasma current. One of the more important influences is the change in plasma major radius growth direction, $\dot{R}_p$, as the beams are applied and is primarily due to the lack of radial position control in these experiments. Another issue is the decrease in electron temperature and confinement time as the beams are injected. In the EC heated plasma the temperature and injected power confinement values are approximately 10 keV and 10 ms, respectively, and are similar to values obtained in normal DIII-D startup with strong EC. However, when beams are injected values decrease substantially. High temperature and good confinement are essential for NB CD efficiency [19] and NB injection into the limited, solenoid-free plasma is seen to reduce both of these parameters. Final I_p decay, starting at 230 ms, indicates the NI CD is insufficient to maintain the plasma current and this is consistent with CD analysis presented below indicating NI current is a small fraction of the total current.

Transport analysis has been carried out using the codes TRANSP [32] and ONETWO [33] with the NUBEAM module [34] to determine the partitioning of various noninductive CD components. Figure 10 shows ONETWO current partitioning results for one of the solenoid-free discharges with two co-directed NBs injected just after solenoid-free flattop ($t =$ 200 ms). EC and NB are shown to provide little noninductive CD. Low NB CD (~10 kA) is associated with excessive loss of fast NB ions due to the low current, low temperature, outside limited plasma. EC contribution is small (<3 kA) and results are consistent with ECCD quantities calculated by the TORAY-GA ray tracing code [35, 36]. The low EC contribution is attributed to the low T_e and ECH resonance located on the low field side of the plasma. The major NI contributor is primarily the bootstrap current (I_{BS}) associated with radial gradients in the T_e profile. The bootstrap current is seen to decrease soon after the current peak/NB initiation and, as seen in figure 9, follows closely the decrease in T_e during the current decay phase. The motion of the plasma towards the outside wall during this period also reduces the overall NI drive.

A second campaign, based on a conventional plasma startup (utilizing the E-coil for inductive initiation) with handoff to DIII-D's primary CD systems: NB, EC and FW was performed to establish information on CD in low current, low temperature, limited plasma typical of that generated by the solenoid-free scenario. A wide range of parameters was varied, including plasma current, beam power, ECH power, density, plasma shape, beam voltage and FW power. Figure 11 shows several plasma current time traces obtained during this campaign. In these experiments, the E-coil is used to provide initial null and flux for plasma initiation and only F6 and F7 are used to provide vertical field and plasma shaping. E-coil current is frozen between 100 and 200 ms (inductive handoff zone) and after 200 ms the current decays with its natural

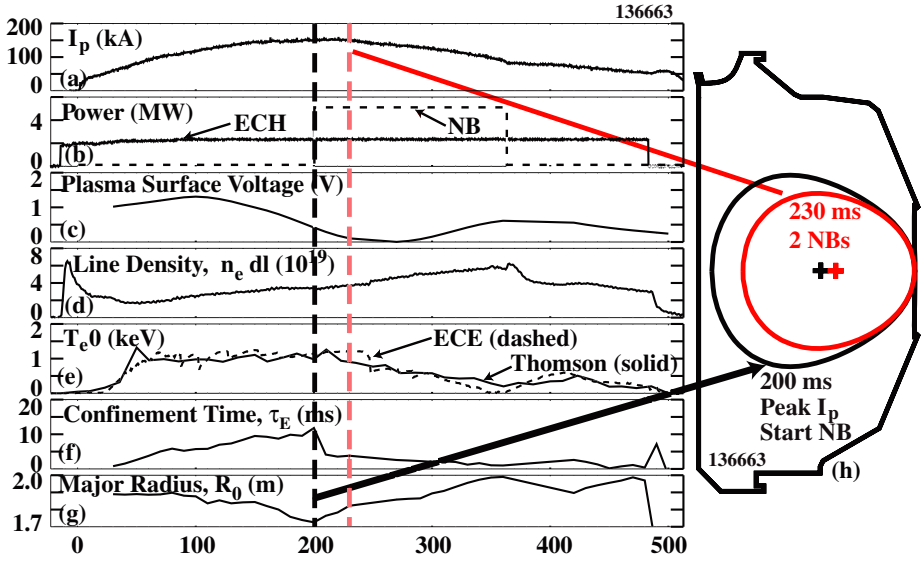

Figure 9. Plasma performance parameters for solenoid-free startup with handoff to two co-left (most tangential) NB at peak current. Shown are (*a*) plasma current, I_p; (*b*) ECH, P_{ECH} and NB, P_{NB} injected power; (*c*) EFIT surface voltage, V_{SURF}; (*d*) line integrated density, $\int n_e\,dl$; (*e*) central electron temperature, $T_e(0)$ from ECE and Thomson scattering diagnostics; (*f*) injected power confinement time, $\tau_E = E_{MHD}/(P_{EC} + P_{NB})$, E_{MHD} = EFIT stored energy and P_{EC} and P_{NB} = ECH and NB injected power, and (*g*) EFIT major radius, R_0. The vertical black dashed line at 200 ms represents peak plasma current, exhaustion of divertor PF coil currents and start of NB injection. The red (grey) dashed line at 230 ms represents parameters typical of those during the NB injection phase. (*h*) EFIT plasma boundary.

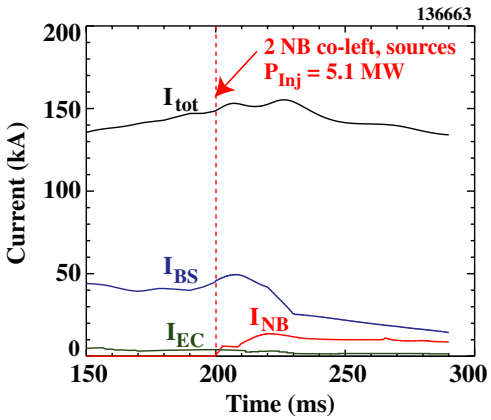

Figure 10. Calculated CD partitioning of the solenoid-free discharge 136663 with two co-left NB sources injected between 200 and 360 ms with total injected power of ∼5 MW. Based on ONETWO [33] with ion beam diffusion of 10 m s^{-2}, set to match experimental stored energy and neutron emission rate. Curves represent: I_{tot} = plasma current; I_{EC} = ECCD; I_{NB} = NBCD; I_{BS} = bootstrap current.

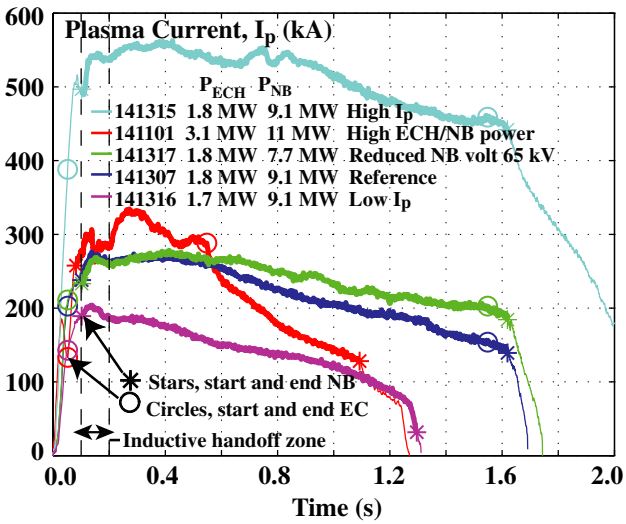

Figure 11. Plasma current time history for a number of discharges using a conventional (E-coil) startup of DIII-D. The E-coil is used to initiate the discharge with its current frozen in the 'inductive handoff zone' (100–200 ms). Various curves show some of the major parameters varied during the campaign. Circles and stars demarcate the beginning and end of the EC and NB power phases of the discharge, respectively. The heavy portions of the line further highlight the NB phase.

L/R time scale, augmented by any noninductive CD provided by NB, EC and FW systems. An inside limited plasma is maintained throughout the discharge in contrast to a normal DIII-D startup, which would divert early in the plasma current ramp-up phase. The ECH and NB phases of each discharge are shown by circles and stars, respectively. The lowest plasma current decay rate plasma (shot 141317) at low current levels ($I_p \sim$ 200–300 kA) was obtained with 4-co beams (3 tangential and 1 normal) at reduced beam voltage of 65 kV (rather than the usual 75 kV) and with 3 of our 6 ECH tubes operational. At higher ECH levels, large MHD, as observed from fast changes in global parameters such as I_p and density, is observed and large minor disruptions significantly decrease performance. FW heating was initiated in several discharges with very little influence on the I_p decay rate. Higher current had only marginal influence on the actual decay rate indicating plasma current at these low values (<600 kA) may not be sufficient to provide improved confinement necessary for steady-state operation in a limited plasma condition. Full sustainment of the plasma current by noninductive means was not observed in any of the discharges. All discharges culminated in a slow L/R decay of the plasma.

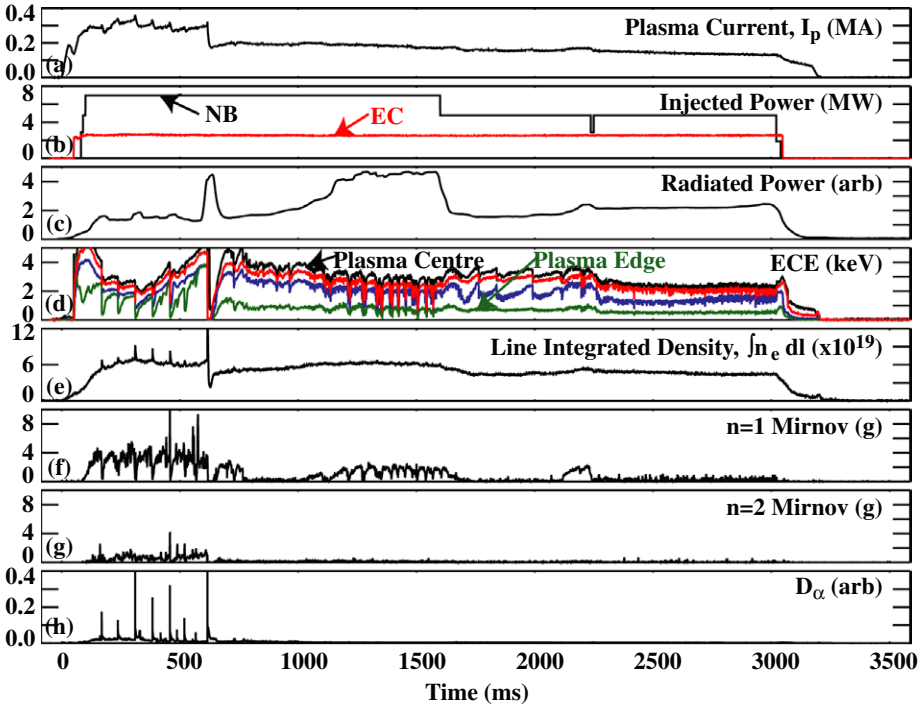

Figure 12. Time history of discharge parameters for conventional startup, limited plasma (141102) with high EC power (five gyrotrons) and large MHD events. Various parameters are (*a*) plasma current, (*b*) NB and EC injected power, (*c*) radiated power, (*d*) ECE showing traces varying from plasma centre to plasma edge, (*e*) line integrated density, $\int n_e\,\mathrm{d}l$, (*f*) rms magnitude $n = 1$ component of Mirnov magnetic probes and (*g*) similar, $n = 2$ component, (*h*) D_α signal from upper outer region of plasma.

Many of the high power discharges contained large MHD disturbances and these significantly modified the overall plasma parameters. Figure 12 shows parameters from a typical discharge with large oscillations in many plasma parameters. This discharge survives what appear to be several minor disruptions including a very large event at ~600 ms. In between these events there seems to be a rise in current and stored energy indicating improved confinement and current overdrive. These results are similar to phenomena observed in standard DIII-D stationary, noninductive ELMing H-mode discharges with high power input and the phenomena has been attributed to collapse of an internal transport barrier (ITB) [19]. The ECE signal (*d*), which estimates the electron temperature at several radial locations across the plasma, is seen to have many small drops in signal with a large drop across the entire plasma seen at 600 ms. The MHD behaviour is seen to have a wide range of mode numbers as shown in the Mirnov signal decomposition into $n = 1$ and 2 components in frames (*f*) and (*g*), respectively. The early MHD signatures are typical of ELM behaviour based on the D_α signal (*h*), and ECE (*d*) showing substantial penetration into the core plasma for these events. Following the large event at 600 ms, MHD activity decreases and a slow decay in plasma current is observed. The current drops typical of that shown in figure 12 are evident in most discharges with high ECH power ($\geqslant$5 gyrotrons) and low density. High density and high NB power ($\geqslant$5 sources), as is present in discharge 141101 (figure 11), reduce the magnitude of the events, but does not arrest the overall L/R decay of the plasma. One potential source of these instabilities is thought to be associated with the very localized heating from focusing all gyrotron tubes (~3 MW) at a single resonant location in the plasma. This single aiming point of the gyrotrons is necessary for initiation of the present DIII-D solenoidless startup, but it is not optimal for noninductive plasma sustainment.

5. Comparison with existing DIII-D CD experiments

Recently, DIII-D has devoted substantial effort towards developing a fully noninductive CD plasma [19, 37–40]. In these experiments, the primary objective is steady-state sustainment of full noninductive current using NB, EC, FW and BS CD methods. All experiments carried out to meet these objectives utilize well-controlled, diverted plasma with H-mode confinement characteristics and target NICD sustainment is in the flat top phase of the discharge. Most experiments are carried out in the mega-Ampere plasma current level where NICD methods are most effective. One noticeable exception to this is an early experiment in DIII-D using eight co-directed hydrogen beams into a helium plasma achieving 340 kA of NICD for of-order 1 s in a well controlled, H-mode quality diverted plasma [18]. Our present six co-/two counter-beam configuration prohibits duplication of these experiments. In contrast, the solenoidless campaign results reported here utilize a marginally controlled, limited plasma with poor transport characteristics. We are attempting to grow a very low current plasma (<200 kA) under very transient conditions with high input power. We require substantial current overdrive to obtain success. It is interesting to compare previous NICD results with those achieved in the present solenoidless campaigns. Figure 13 shows the plasma current wave forms for a number of noninductive discharges achieved in DIII-D along with some of those achieved in the

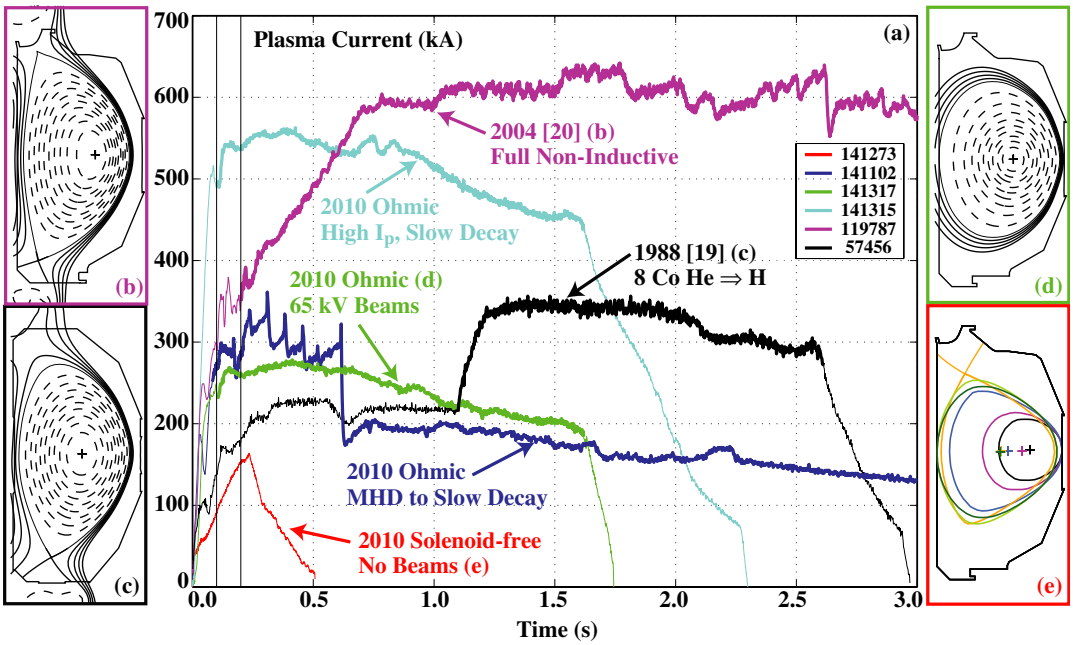

Figure 13. Comparison of existing DIII-D noninductive plasma current wave forms with those generated during the solenoid-free campaign. (*a*) Plasma current time history comparison for some of DIII-D's NI discharges [18, 19] along with selected discharges from the 2009–2010 solenoid-free campaign. (*b*) The divertor shape used in the recent DIII-D NICD experiment [19], (*c*) the divertor shape achieved in the earlier H into He experiments [18], (*d*) the limited circular plasma utilized in the 2010 ohmic transition to noninductive operation and (*e*) several plasma boundaries achieved during a typical solenoid-free initiation.

solenoidless campaign. In recent experiments, sustainment at 600 kA was attained, although the current profiles were still evolving at the end of the discharge [19]. In contrast, the solenoidless campaign discharges all had a slow decay in plasma current. Even at the current levels comparable to recent DIII-D shots with self-sustaining current levels (∼600 kA), the limited plasma studied in these campaigns were not self-sustaining. The primary shape difference, diverted versus limited, as contrasted in the left versus right plasma shapes shown in figure 13, is believed to be a large contributor to the lack of sustainment in the solenoidless campaign. It is expected that diverted plasma is highly desirable for achieving solenoid-free current sustainment and future experiments in this area are expected to utilize configurations similar to those that have achieved successful NICD.

6. Conclusions

A solenoid-free startup to 166 kA of plasma current has been achieved using only PF coils located outside the centrepost region of DIII-D. With sufficient EC heating, the developed scenario efficiently converts flux to plasma current with efficiency similar to conventional ECH assisted E/F coil startup ($C_{\mathrm{Ejima}} \sim 0.3$). Pulse extension to 800 ms has been achieved with radial position control. Requirements of the present DIII-D PS systems dictate that the final plasma is a limited circular plasma, although diverted plasmas are produced transiently during the initiation phase. Preliminary investigations were carried out to determine potential for noninductive CD in solenoidless plasmas and in a limited plasma generated using the standard DIII-D startup. A wide range of plasma parameters was investigated using DIII-D's conventional startup. Large MHD activity was observed for large EC power injected into small current, limited plasma discharges and this significantly limits plasma performance. Best discharge performance (i.e. lowest plasma decay rate) was obtained with moderate ECH and NB power, but full noninductive, steady-state sustainment of the limited, low current plasma was not achieved. Further development of the solenoid-free startup on DIII-D is possible, with best NICD results expected if diverted H-mode quality plasma can be achieved.

Acknowledgment

This work was supported by the US Department of Energy under DE-FC02-04ER54698, DE-AC02-09CH11466, DE-FG02-07ER54917 and DE-AC05-00OR22725.

References

[1] Stambaugh R.D. *et al* 2011 *Fusion Sci. Technol.* **59** 279
[2] Peng Y.K.M. *et al* 2009 *Fusion Sci. Technol.* **56** 957
[3] Ono M. *et al* 1993 *Proc. 14th Int. Conf. on Plasma Phys. Control. Nucl. Fusion Research 1992 (Wurzburg, Germany 1992)* vol 1 (Vienna: IAEA) p 693 (http://www-naweb.iaea.org/napc/physics/PS/publications/pub_nf.htm)
[4] Raman R. *et al* 2007 *Nucl. Fusion* **47** 792
[5] Battaglia D. *et al* 2009 *Phys. Rev. Lett.* **102** 225003
[6] Shevchenko V.F. *et al* 2010 *Nucl. Fusion* **50** 022004
[7] Jackson G.L. *et al* 2010 DIII-D experimental simulation of ITER scenario access and termination *Proc. 23rd IAEA Conf. on Fusion Energy (Daejeon, South Korea, 2010)* (Vienna: IAEA) EXS/P2-11 and http://www-pub.iaea.org/MTCD/Meetings/PDFplus/2010/cn180/cn180_papers/exs_p2-11.pdf
[8] Sykes A. *et al* 2001 *Nucl. Fusion* **41** 1423

[9] Gryaznevich M. *et al* 2006 *Nucl. Fusion* **46** s573
[10] Takase Y. *et al* 2002 *J. Plasma Fusion Res.* **78** 719
[11] Ushigome M. *et al* 2006 *Nucl. Fusion* **46** 207
[12] Forest C.B. *et al* 1992 *Phys. Rev. Lett.* **68** 3559
[13] Forest C.B. *et al* 1994 *Phys. Plasma* **1** 1568
[14] Taoka H. *et al* 2000 *J. Plasma Fusion Res.* **76** 561
[15] Mitarai O. *et al* 2004 *J. Plasma Fusion Res.* **80** 549
[16] Mitarai O. *et al* 2010 *J. Plasma Fusion Res.* **9** 100
[17] Raman R. *et al* 2010 *Phys. Rev. Lett.* **104** 095003
[18] Simonen T.C. *et al* 1988 *Phys. Rev. Lett.* **61** 1720
[19] Politzer P.A. *et al* 2005 *Nucl. Fusion* **45** 417
[20] Luxon J.L. *et al* 1985 *Fusion Technol.* **8** 441
[21] Lloyd B. *et al* 1991 *Nucl. Fusion* **31** 2031
[22] Hong R. *et al* 1987 *Proc. 12th Symp. on Fusion Engineering and Design* vol 2, p 1133
[23] Lohr J. *et al* 2009 *Proc. 34th Int. Conf. on Infrared, Millimeter, and Terahertz Waves 2009 (Busan, South Korea, 2009)* and http://ieeexplore.ieee.org/xpl/freeabs_all.jsp?arnumber=5324618
[24] Pinsker R.I. *et al* 2009 *AIP Conf. Proc.* **1187** 77
[25] Leuer J.A. *et al* 2010 *Fusion Sci. Technol.* **57** 48
[26] Leuer J.A. *et al* 2010 *IEEE Trans. Plasma Sci.* **38** 333
[27] Leuer J.A. *et al* 1993 *Proc. 15th IEEE/NPSS Symp. on Fusion Engineering 1993 (Hyannis, MA,1993)* vol 2 (Piscataway, NJ: IEEE) p 629 (http://ieeexplore.ieee.org/iel2/3943/11419/00518409.pdf)
[28] Lazarus E.A. *et al* 1998 *Nucl. Fusion* **38** 1083
[29] Mukhovatov V.S. and Shafranov V.D. 1971 *Nucl. Fusion* **11** 605
[30] Ejima S. *et al* 1982 *Nucl. Fusion* **22** 1313
[31] Lao L.L. *et al* 1985 *Nucl. Fusion* **25** 1421
[32] Hawryluk R.J. 1980 *Physics Close to Thermonuclear Conditions* vol 1 (Brussels: Commission of the European Communities) p 19
[33] St John H.E. *et al* 1995 *Proc. 15th Int. Conf. on Plasma Phys. Control. Nucl. Fusion Research 1994 (Seville, Spain, 1994)* vol 3 (Vienna: IAEA) p 603 (http://www-naweb.iaea.org/napc/physics/PS/publications/pub_nf.htm)
[34] Pankin A. *et al* 2004 *Comput. Phys. Commun.* **159** 157
[35] Kritz A.H. *et al* 1982 *Proc. 3rd Int. Symp. on Heating in Toroidal Plasmas 1982 (Grenoble, France, 1982)* vol II (Brussels: ECE) p 707
[36] Lin-Liu Y.R. *et al* 2003 *Phys. Plasmas* **10** 4064
[37] Greenfield C.M. *et al* 2003 *Proc. 30th European Phys. Soc. Conf. on Controlled Fusion and Plasma Physics (St Petersburg, Russia, 2003)* vol 27A (ECA) P-4.92 and http://epsppd.epfl.ch/StPetersburg/PDF/P4_092.PDF
[38] Murakami M. *et al* 2006 *Phys. Plasmas* **13** 056106
[39] Murakami M. *et al* 2005 *Nucl. Fusion* **45** 1419
[40] Ferron J.R. *et al* 2011 Optimization of the safety factor profile for high noninductive current fraction discharges in DIII-D *Nucl. Fusion* accepted